Science of the Total Environment 794 (2021) 148714

Contents lists available at ScienceDirect

Science of the Total Environment

journal homepage: www.elsevier.com/locate/scitotenv

Enhancing effect of NO_2 on the formation of light-absorbing secondary organic aerosols from toluene photooxidation

Shijie Liu [a], Yiqian Wang [a], Gehui Wang [a,b,*], Si Zhang [a], Dapeng Li [a], Lin Du [c], Can Wu [a], Wei Du [a], Shuangshuang Ge [d]

[a] Key Lab of Geographic Information Science of the Ministry of Education, School of Geographic Sciences, East China Normal University, Shanghai 210062, China
[b] Institute of Eco-Chongming, 3663 North Zhongshan Road, Shanghai 200062, China
[c] Environment Research Institute, Shandong University, Qingdao 266237, China
[d] Institute of Urban Meteorology, China Meteorological Administration, Beijing 100089, China

HIGHLIGHTS

- A chamber study of the effect of NO_2 on the toluene SOA formation through OH-oxidation
- The MAC value of toluene-derived SOA continuously increased with increasing NO_2 concentration.
- The evolution characteristics of the toluene SOA chemical compositions were studied by the HR-ToF-AMS.
- Nitro compounds play an important role in the enhance of MAC value at high NO_2 condition.

GRAPHICAL ABSTRACT

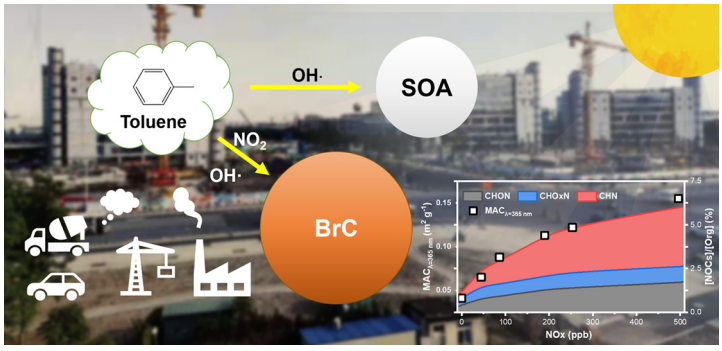

ARTICLE INFO

Article history:
Received 24 March 2021
Received in revised form 23 June 2021
Accepted 23 June 2021
Available online 27 June 2021

Editor: Pingqing Fu

Keywords:
Brown carbon
Photooxidation
Toluene
NO_2
Nitrogen-containing organic compounds

ABSTRACT

Aromatic hydrocarbons are one of the major precursors of atmospheric brown carbon (BrC) and both abundantly co-exist with NO_x in the urban atmosphere especially in winter haze period. However, the impact of NOx on the formation of BrC derived from aromatic hydrocarbons is still not fully understood. In this study, the yield and light absorption of secondary organic aerosols (SOA) from toluene photooxidation under various nitrogen oxides (NO_2) levels were investigated by using a 5 m^3 photooxidation smog chamber. A trend of increase at first and then decrease in the SOA yield with an increasing NO_2 concentration was observed. The acid-catalyzed heterogeneous reactions lead to the increase of SOA yield in the low-NO_2 regime. The formation of low-volatility species might be suppressed at high-NO_2 conditions is responsible for the decreased SOA yield. In contrast, light absorption and mass absorption coefficient (MAC) of the toluene-derived SOA continuously increased with the increasing NO_2 concentrations. HR-ToF-AMS results showed that nitrogen-containing organic compounds (NOCs) are the main species that lead to the increase of the SOA light absorption. The ratio of CHN family to the total NOCs, which are derived from the nitro compounds, also increased dominantly with the increasing NO_2 levels and accounted for more than half of the total NOCs when the NO_2 concentration increased to 495 ppbv, indicating that nitro compounds rather than organic nitrates are the major light-absorbing species and preferably formed in the toluene oxidation process.

* Corresponding author at: Key Lab of Geographic Information Science of the Ministry of Education, School of Geographic Sciences, East China Normal University, Shanghai 210062, China.
E-mail address: ghwang@geo.ecnu.edu.cn (G. Wang).

https://doi.org/10.1016/j.scitotenv.2021.148714
0048-9697/

1. Introduction

Atmospheric brown carbon (BrC) is a class of particulate organic compounds with an exponentially increasing absorption in the light spectrum from the visible to ultraviolet (UV) wavelength, which has been observed from the ground surface to the free troposphere (Ma et al., 2019; Wu et al., 2020). Remote sensing observations and chemical transport model simulation results showed that the global direct radiative forcing of BrC ranges from 0.1 to 0.6 $W m^{-2}$, suggesting its potential climate forcing importance (G.X. Lin et al., 2014; Zhang et al., 2017). BrC is only second to black carbon (BC) on the warming effect of particulate matter in the atmosphere (Laskin et al., 2015; Y.H. Lin et al., 2014; Wang et al., 2018; Zhang et al., 2020). A few studies reported that the contribution of BrC to aerosol forcing can account for around a fifth of the solar absorption of carbonaceous aerosols globally (Chung et al., 2012; Peng et al., 2020; Xie et al., 2017). Due to its effective absorption of UV irradiation at the wavelength of $\lambda < 320$ nm, BrC can suppress ozone photolysis and the production of OH radicals, and consequently affect the atmospheric photochemistry (Jo et al., 2016; P.F. Liu et al., 2015).

BrC in the atmosphere is originated primarily from the direct emissions of incomplete combustion of biomass and fossil fuel and secondarily from photochemical reaction of VOCs with anthropogenic pollutants such as NOx ($NO_2 = NO + NO_2$), O_3, SO_2 and NH_3. Dark and photochemical processes of the aqueous-phase reactions can promote the optical spectra of organic aerosols, and are also the important process of secondary BrC formation (Y. Chen et al., 2020; Huang et al., 2018; Slikboer et al., 2015; Xu et al., 2018). Formation and light absorption of BrC are affected by many environment factors such as concentrations and compositions of VOCs and oxidants, aerosol aqueous phase acidity, and meteorological conditions. In the past decades, field observation on BrC have been conducted in various regions, but the formation mechanisms of BrC are not yet clarified and thus knowledge about the relationship between the chemical compositions and the optical properties of BrC remains limited, because of the diversity of VOCs, oxidation reactions and influencing factors and the complexity of secondary BrC compositions (Q.Y. Wang et al., 2019; Yan et al., 2020).

Aromatic hydrocarbons and NO_x are the major gaseous pollutants in the winter atmosphere of China and co-abundantly occur with BrC in Chinese haze development process (Wang et al., 2016). Recently, a few field measurements have investigated the association between BrC and NO_2 in Chinese haze periods. For example, Peng et al. (2020) evaluated the light absorption of BrC in filter-based $PM_{2.5}$ samples collected in the Sichuan Basin of Southwest China and found that BrC absorption was significantly higher during the pollution period over the clean period, and a large amount of BrC formed on the polluted days was related to the aqueous phase reactions of NO_2 with anthropogenic precursors (Peng et al., 2020). X.R. Li et al. (2020) examined the light absorption properties of BrC collected in northwest China during winter and found that there was evident correlation between the absorption coefficients (Abs) of BrC and NO_2, which suggested an important contribution of nitrated aromatic compounds to light absorption (J. Li et al., 2020). Recent research also illustrated that the formation of a moderately oxidized oxygenated organic aerosol (MD-OOA) with nitrogen components is responsible for the increasing light absorption (Wang et al., 2021). The effects of NO_2 on secondary BrC formation were also studied in laboratory studies. A scientific assessment on the optical role of BrC by Y.C. Liu et al. (2015) indicated that the wavelength-dependent absorptive component (k) values of secondary organic aerosols (SOA) formed in the presence of NO_2 are greater than those without NO_2, and the nitrogen-containing organic compounds (NOCs) are the key components enhancing light absorption (Y.C. Liu et al., 2015). Xie et al. (2017) reported that the light absorption of SOA generated in the presence of NO_2 is higher than that of hydrogen peroxide (H_2O_2), and the mass absorption coefficient (MAC) of nitro-aromatic compounds is more than twice as that of the whole SOA at 365 and 400 nm (Xie et al., 2017). Lin et al. (2015) compared the $MAC_{\lambda=365\ nm}$ of toluene SOA under a high- and a low-level of NO_2 conditions, and found that $MAC_{\lambda=365\ nm}$ increased about 80 fold when the initial concentration ratio of NO_2 to toluene ($[NO_2]_0/[toluene]_0$, ppbv $ppbv^{-1}$) changed from 1:300 to 1:2 (Lin et al., 2015). The above field and laboratory studies suggested that NOx could promote BrC formation. However, the detailed dynamics of impact of NOx levels on BrC formation is still not fully understood especially on a molecular level.

Toluene is one of the most abundant aromatic VOCs in the urban atmosphere, which is also an important source of BrC (Laskin et al., 2010; Ma et al., 2018). In the present study, the formation dynamics and light absorbance of SOA formed from the photooxidation of toluene were investigated with the initial NO_2 concentrations varied from 0 to 500 ppbv. In complement to the optical measurements, the SOA chemical composition was also characterized by using a *high-resolution time-of-flight aerosol mass spectrometer* (HR-ToF-AMS) for identification of the whole SOA chemical composition. The possible products with UV absorbance were elucidated. We found that the increase of SOA light absorption was related to the concentration of NOCs, and nitro-aromatic compounds with higher absorbance are dominantly formed under higher NO_2 conditions compared to other kinds of NOCs.

2. Experimental methods

2.1. Chamber studies

The secondary BrC was formed in a 5 m^3 Smog Chamber of East China Normal University. The method for SOA formation in the chamber followed the procedures given in our previous studies (Ge et al., 2019; Liu et al., 2017; Liu et al., 2019). A summary of experimental conditions for the photooxidation of toluene is provided in Table 1. The concentrations of toluene and NO_2 in the experiments were higher than those in the real atmosphere to keep the particle production significant enough for off-line collections and accurate measurements. The toluene concentrations remained stable in the different experimental conditions, the variation of toluene-derived SOA mass concentration and yield was only affected by the NO_2 concentration in this study. The $[toluene]_0/[NO_2]_0$ ratios in this study covered the atmospheric conditions from clean to polluted (Han et al., 2015; Zou et al., 2015). The experimental conditions informative to aerosol formation and in the atmosphere pollution degree. All experiments were performed at 1 atm, and the temperature inside the chamber was kept at 298 ± 2 K. Before each experiment, the chamber was flushed by zero air for more than 24 h until the number of particles inside the chamber was less than 5 cm^{-3} and the concentrations of NO_2 and O_3 were lower than1 ppbv, respectively. While being flushed, the chamber was continuously irradiated with the UV lights to completely remove organics potentially absorbed on the inside surface of the chamber. Zero air was generated through a Zero Air Supplier (111-D3N, Thermo Scientific™, U.S.A.) and the flow rate was regulated by a mass flow controller (D088C/ZM, Beijing Sevenstar Electron Corporation). The relative humidity (RH) of the zero air was about 15–20%. The OH radicals were generated by H_2O_2 photolysis under UV light (TUV36W, Philips) irradiation. NO_2 (510 ppm in N_2, Air Liquid Shanghai, China) was introduced into the chamber directly from the corresponding standard gas cylinders. For each experiment, the same amounts of toluene (EMD Chemicals, ≥99.8%) and H_2O_2 (Sigma-Aldrich, 30 wt% in H_2O) solution were injected into a Teflon tube and gently blown into the chamber by the zero air. The injected toluene concentration was 520 ppbv and the H_2O_2 concentration was 900 ppbv, which were calculated from the injection volume of the liquids. The wall loss rate constant of the particles mass concentration was (4.7 ± 0.3) × 10^{-5} s^{-1}, and the measured particle concentrations and SOA yield in this study were corrected by the wall loss rate in the same way as reported in our early study (Liu et al., 2017). Each experiment was performed without seed aerosols here. The photooxidation started when the UV light was turn on, and each experiment lasted for about 3 h.

Table 1
Details on the experimental conditions for the photooxidation of the toluene/OH system.

Exp. no.	Toluene (ppbv)	H_2O_2 (ppbv)	$[NO_2]_0$ (ppbv)	SOA ($\mu g.m^{-3}$)	SOA yield
1	520	900	~0	74.3	3.4%
2	520	900	44.6	111.8	5.2%
3	520	900	86.2	115.5	5.3%
4	520	900	101.3	146.4	6.8%
5	520	900	153.3	135.7	6.3%
6	520	900	189.9	126.8	5.9%
7	520	900	253.5	123.2	5.7%
8	520	900	496.2	112.8	5.2%

2.2. Sample collection

The formed toluene SOA was collected onto Teflon filters (Whatman, 0.2 μm PTFE 46.2 mm Filter) at the end of each experiment and measured for the light absorption. Of note, in order to investigate the bleaching effect on BrC, the SOA was collected as soon as it was detected by A scanning mobility particle sizer (SMPS), and was defined as newly formed SOA in this study. By comparison, the SOA collected at the end of each experiment with an average photooxidation time of 2 h was defined as aged SOA. The toluene SOA was collected at a flow rate of 30 L min^{-1} for 2 h, and the sampling volume was 3.6 m^3. The filter was extracted with 10 mL of methanol (HPLC grade, Sigma-Aldrich) for 10 min under sonication. Then the extracts were filtered through a 0.45 μm syringe filter (Fisher Scientific, Fisherbrandt Syringe Filters) to remove the insoluble components and determined for light-absorbance.

2.3. Experimental equipment

An online NOx analyzer (Model 42i, Thermo Scientific™, U.S.A.) was used for the NO_2 measurement. The uncertainty of the NO_2 measurement was less than ±1%, and the detection limits of NO_2 analyzer were 0.40 ppbv. Both RH and temperature were measured with an Omega digital thermohydrometer (model RH411, Omega Engineering, Inc., Stamford, CT).

The number concentrations and size distributions of SOA were determined by the SMPS, which consists of a differential mobility analyzer (DMA model 3081, TSI Inc., U.S.A.) and a condensation particle counter (CPC model 3776, TSI Inc., U.S.A.) for the particle size screening and particle number concentration determination, respectively. A sheath/sample flow relationship of 3.0/0.3 L min^{-1} in the DMA was used for the measurements. To make sure all the particles could be detected, each scan was 240 s and the particle size was obtained in the range of 14 to 710 nm. The mass concentration was converted from the particle volume concentration with a material density. For toluene-derived SOA, the material density measured by Ng et al. is 1.4 ± 0.1 g cm^{-3} (Ng et al., 2007), which is used in this study for the related calculations.

Realtime chemical composition of toluene SOA was measured using an Aerodyne high-resolution time-of-flight aerosol mass spectrometer (HR-ToF-AMS; Aerodyne Research Inc. U.S.A.). V-mode ($m/\Delta m$ = ~2000), which has a higher signal-to-noise ratio, was used in the AMS ToF section. The operation protocols of the AMS are briefly described as follows. First, the particles with an aerodynamics diameter less than 1 μm were focused into a narrow beam through an aerodynamic lens, subsequently impacted onto the hot tungsten surface (~600 °C) inside the AMS and were vaporized. Then, the vaporized species were ionized by electron ionization (EI), of which the energy of ionization was 70 eV. The composition dependent collection efficiency (CE) was applied to the data based on Middlebrook et al. (2012). Default relative ionization efficiency (RIE) values were used for the HR-ToF-AMS data. The AMS data were analyzed by using the standard AMS data analysis toolkits SQUIRREL v1.53C coupled with PIKA 1.12C (http://cires.colorado.edu/jimenez-group/ToFAMSResources/ToFSoftware/index.html) based on Igor Pro 6.32A (WaveMetrics Inc.). The RIE values of sulfate, nitrate, chloride and organic was 1.0, 1.1, 1.3 and 1.4 for the mass concentration calculations, respectively.

2.4. UV–Vis light absorption analyses

The UV–Vis light absorption spectra of toluene SOA with different NO_2 concentrations were measured by a UV–Vis spectrophotometer (UV-3600, Shimadzu, Japan) with a 1 cm cuvette at wavelength range of 200–800 nm. The UV–Vis spectra were collected with a resolution of 0.5 nm^{-1}. The detailed method was described in previous studies (J. Li et al., 2020; Yan et al., 2020). Light absorption coefficient of the particles at a specific wavelength λ (Abs_λ, M/m) was calculated as Eq. (1) below:

$$Abs_\lambda = (A_\lambda - A_{700}) \cdot \frac{V_l}{V_a \cdot L} \cdot \ln(10) \quad (1)$$

where Abs_λ is the light absorption of SOA at the λ wavelength, A_{700} is the light absorption intensity background value (in order to reduce the limits of error in measurement, the average value of light absorption intensity of 695–705 nm was used as A_{700}), V_l is the volume of methanol with dissolved aerosols, V_a is the volume of the sampled air, and L (1 cm) is the optical path length. The limit of detection (LOD) was 0.081 M/ m in the 300–700 nm wavelength range with an estimated uncertainty of 21%. Since the measured Abs_λ is strongly dependent on the amount of SOA collected on the filter, mass absorption coefficient (MAC, $m^2\ g^{-1}$) was used here for a comparison, which was calculated using Eq. (2) below:

$$MAC_\lambda = \frac{Abs_\lambda}{M} \quad (2)$$

where MAC_λ is the mass absorption coefficient of SOA at the λ wavelength, M (μg m^{-3}) is the mass concentration of methanol-soluble organic matter.

3. Result and discussion

3.1. Effect of NO_2 on toluene-derived SOA formation

To investigate the role of NO_2 in the toluene SOA formation by OH oxidation, a series of photooxidation experiments were conducted with the initial NO_2 concentration ranging from 0 to 496.2 ppbv. The temporal evolution of SOA formation as a function of reaction time under different initial NO_2 concentrations is shown in Fig. 1. The new particles formed in the chamber were observed after 10 min UV-irradiation (Fig. 1a). Then the SOA mass concentration gradually increased as the irradiation proceeded. After about 1 h of photooxidation, the SOA concentration was stable as it reached the maximum, which means that the photooxidation was almost completed and no additional SOA was formed any more. SOA yield was used to represent the SOA formation potential in the photooxidation process. In this work the SOA yield was calculated as follows:

$$Y = \frac{\Delta M_0}{\Delta HC} \quad (3)$$

where Y is the SOA yield, ΔM_0 is the maximum concentration of organic aerosols in the chamber (μg m^{-3}), and ΔHC is the concentration of reacted toluene (μg m^{-3}).

Fig. 1b shows the changes in the maximum concentration of SOA and SOA yields of toluene at different NO_2 concentrations. There was an increase at first and then decrease in the SOA yield with the increasing NO_2 concentration. The SOA maximum concentration was 74.3 ±

2.3 μg m^{-3} in the absence of NO_2, and increased to a maximum of 146.4 ± 1.8 μg m^{-3} when the initial NO_2 increased to 101.3 ppbv. Afterwards, the SOA maximal concentration decreased gradually to 112.9 ± 2.4 μg m^{-3} as initial NO_2 reached 496.2 ppbv. The toluene SOA yield was 3.4%, 6.8% and 5.2% when the initial NO_2 concentration was ~0, 101.3, and 496.2 ppbv, respectively. The maximum of SOA yield was observed when concentration ratio of $[NO_2]_0/[toluene]_0$ was about 1:5. Such a variation pattern in SOA growth rate of increasing under relatively low NO_2 conditions and decreasing under relatively high NO_2 conditions was also observed by previous studies. Sarrafzadeh et al. (2016) and Qi et al. (2020) pointed out that the promotion of NO_2 on SOA formation was due to the increase of OH concentration in the chamber (Qi et al., 2020; Sarrafzadeh et al., 2016). However, both studies were conducted under black light irradiation conditions with a light wavelength of 365 nm, and the OH was generated through recycling via $(NO+NO_2)$/HOx chemistry. UV light in the wavelength of 254 nm was used in this study. Thus, the OH was formed from H_2O_2 photolysis directly, and the OH formation was almost unaffected by NO_2. Therefore, although the same change trend was observed in our and the previous studies, the mechanism of NO_2 affecting SOA formation should be different.

NO^+ and NO_2^+ are the main fragments of both organic and inorganic nitrates detected by AMS, but the NO^+/NO_2^+ ratio is different between the two types of nitrates. NO^+/NO_2^+ ratio of organic nitrates is substantially higher than ammonium nitrates (Boyd et al., 2015). Thus, NO^+/NO_2^+ ratio in the AMS mass spectra is routinely used to distinguish the organic nitrates from inorganic nitrates (Farmer et al., 2010; Ng et al., 2017; L. Xu et al., 2015), and the NO_{org} and $NO_{2,org}$ concentrations can be calculated by using the following equations:

$$NO_{2,org} = \frac{NO_{2,meas} \times (R_{meas} - R_{AN})}{R_{ON} - R_{AN}} \quad (4)$$

$$NO_{org} = R_{ON} \times NO_{2,org} \quad (5)$$

where R_{meas} is the NO^+/NO_2^+ ratio from the observation. R_{AN} is the NO^+/NO_2^+ ratio for ammonium nitrate (AN). The value of 1.3 ± 0.1 was used in calculations for R_{AN} in our AMS data, which is within the range (1.1–3.5) reported in literatures (Farmer et al., 2010; Fry et al., 2013; Ng et al., 2017). R_{ON} is the NO^+/NO_2^+ ratio for organic nitrates. In this work, the NO^+/NO_2^+ ratio of organic nitrates from the photooxidation of aromatic hydrocarbons is 4.8 ± 1, which is much higher than that of ammonium nitrate (Sato et al., 2010). $NO_{2,meas}$ represents the total NO_2^+ fragments obtained from the AMS data.

The mass concentration ratio of nitrate ions to SOA ($[NO_3^-]/[Org]$) obtained by the AMS under different initial NO_2 concentrations is shown in Fig. 2. With the increase of initial NO_2 concentration in the chamber, an increase in the $[NO_3^-]/[Org]$ ratio was observed, suggesting more inorganic nitrate was formed under higher NO_2 conditions. Since inorganic acid could catalyze particle-phase heterogeneous reactions of organic carbonyl species and lead to an increase in SOA mass (Jang et al., 2002), the higher ratio of $[NO_3^-]/[Org]$ observed in this work suggests an increase in acidity of the secondary aerosols along with an increasing NO_2 concentrations, which is responsible for the acid-catalyzed reactions and the promotion of SOA formation.

The chemical composition of toluene-derived SOA in terms of H/C and O/C ratios at different initial NO_2 concentration was further compared. The elemental ratios of O/C vs. H/C for different initial NO_2 concentrations are shown in Fig. 3a. The slope of the linear fit of H/C vs. O/C of toluene-derived SOA at different initial NO_2 concentrations in the Van Krevelen diagram is used to illustrate the chemical processes involved in the evolution of SOA (Heald et al., 2010). The fitted slope for toluene SOA at different conditions is shown in Fig. 3b. The slop of the linear fit of H/C vs. O/C of toluene-derived SOA was about −2.3 in the absence of NO_2. The slop increased quickly to −1.5, −1.3 and −0.97 as the initial NO_2 concentration increased to 45, 86 and 190 ppb, respectively, which indicated that the growth rate of O atoms in SOA formation process was increased with initial NO_2 concentrations. Previous studies found that the glyoxal and methylglyoxal were formed from the toluene OH-oxidation, and exhibits high O/C ratios (Ji et al., 2017). The hemiacetal and acetal formation through the acid-catalyzed reactions resulted in the participation of glyoxal into the particle phase (Jang et al., 2002). Hence, the decrease slop of H/C vs. O/C was observed. The similar decreased trend of the H/C vs. O/C slop was evidenced through acid-catalyzed heterogeneous uptake based on the data in a previous study (Chhabra et al., 2011; Zhao et al., 2018).

In addition, the formed HNO_3 could promote the formation of some compounds with high oxidation state and low volatility (Connelly et al., 2012), which is another reason for the increase of SOA yield with the increasing NO_2 concentrations. Previous studies found that the initial reaction of toluene with OH radicals is a OH addition pathway, which results in the formation of the OH-toluene adduct (e.g., methylhydroxycyclohexadienyl radicals) (Ji et al., 2017). In addition, O_2 addition to the OH-toluene adducts would form the primary RO_2 radicals and subsequently form glyoxal and methylglyoxal through

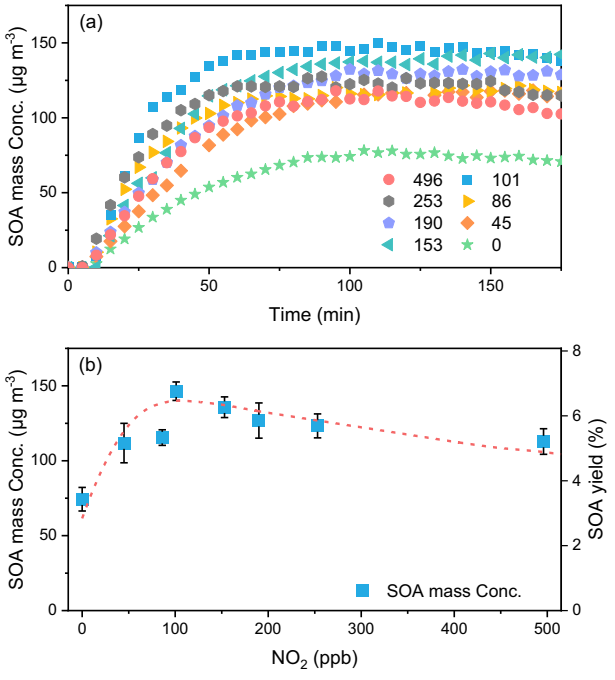

Fig. 1. The temporal evolution of the formed toluene SOA (a) and the maximal SOA mass concentration (b) with different NO_2 concentrations (All the data were corrected for the wall loss).

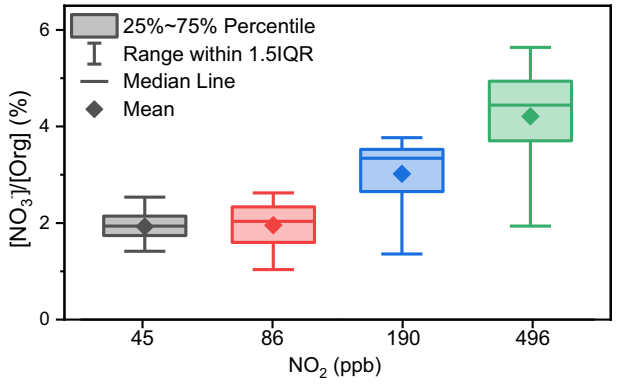

Fig. 2. Concentration ratio of nitrate to SOA ($[NO_3^-]/[Org]$) at different initial NO_2 concentrations.

a ring cleavage reaction. Both carbonyls are further oxidized into glyoxylic acids in the presence of nitric acid (Connelly et al., 2012).

Although only NO_2 was introduced into the chamber before the photooxidation, the NO could be formed through the NO_2 photolysis under the UV light irradiation and the glyoxylic acid formation. With the continuous increase of NO_2 or nitric acid, more NO was formed in the chamber. Then, the reaction of NO with RO_2 would be promoted, and gradually replace the reaction of RO_2 with RO_2/HO_2 (Liu et al., 2019; Xu et al., 2020; Zhao et al., 2018). The reaction of RO_2 with NO could lead to fragmentation by RO intermediate, then produce more higher volatile compounds and thus reduce the formation of SOA (Hu et al., 2007; J.L. Xu et al., 2015). As shown in Fig. 3a, SOA formed at high NO_2 has a lower H/C compared to that at low NO_2. Zhao et al. (2018) pointed the organic nitrates formed through RO_2 reacted with NO have a lower H/C ratio than hydroperoxides, which was formed from the RO_2 reacted with HO_2 at low NOx condition (Zhao et al., 2018). The decrease of H/C observed with the increase of initial NO_2 condition illustrated that the contribution reaction of RO_2 with NO was enhanced with NO_2 concentration. However, it should be noted that despite a descending trend of SOA mass concentration was observed with the continuous increase of initial NO_2 concentration, the SOA mass concentration with 496.2 ppbv initial NO_2 was still 1.5 times higher than that in the absence of NO_2.

3.2. Light absorption of toluene derived SOA

Both Abs and $MAC_{\lambda=365\ nm}$ were used to investigate the effect of NO_2 on the light absorption of toluene-derived SOA in the chamber. The measured Abs and the calculated $MAC_{\lambda=365\ nm}$ with different initial NO_2 concentrations are shown in Fig. 4. As seen in Fig. 4a, light absorption of the toluene derived SOA in the chamber increased along with an increase in NO_2 concentration in the wavelength range from 200 nm to 500 nm. As shown in Fig. 4b, $MAC_{\lambda=365\ nm}$ of the toluene derived SOA formed through OH oxidation was 0.041 $m^2\ g^{-1}$ in the absence of NO_2 and increased to 0.155 $m^2\ g^{-1}$ when the initial concentration of NO_2 increased to 496.2 ppbv, further suggesting that the increase of NO_2 concentration not only promoted the SOA production but also enhanced the light-absorbing ability of SOA formed in the chamber.

Such an increase of MAC with NO_2 is in a good agreement with those reported by Lin et al. (2015) and Xie et al. (2017), but there is a great deal of difference among the MAC values (Table 2). Lin et al. (2015) reported that $MAC_{\lambda=365\ nm}$ of toluene SOA formed at high NO_2 condition was 0.78 $m^2\ g^{-1}$, but the toluene SOA produced without NO_2 was colorless with the value of $MAC_{\lambda=365\ nm}$ being 0.01 $m^2\ g^{-1}$. First, NO_2 in the study of Lin et al. was 1500 ppbv, and the concentration ratio of NO_2 to toluene was 5:1; both are much higher than those of this study. Secondly, BrC is chemically unstable and the chromatic groups can be degraded by extra oxidants, or the bleaching effect may also be induced by direct photolysis (Y.C. Liu et al., 2015). A shorter wavelength of 254 nm UV lights used in this study compared to the study by Lin et al. (2015), which may cause an enhancing bleaching effect and thus result in the lower MAC values compared to that observed by Lin et al. (2015). As seen in Fig. 4b, the average $MAC_{\lambda=365\ nm}$ of the toluene SOA with 2 h of photooxidation was about 40% lower than that of the newly formed SOA. For a better comparison about the influence of NO_2 on the toluene SOA absorption, the relation of $MAC_{\lambda=365\ nm}$ with NO_2 concentration in different studies was shown in Fig. 5. As seen Fig. 5, the increase rate of $MAC_{\lambda=365\ nm}$ with initial NO_2 concentration for the newly formed SOA in this study (slope $= 5.0 \times 10^{-4}$) was comparable to that observed by Lin et al. (slope $= 5.1 \times 10^{-4}$). Therefore, it can be assumed that the bleach effect in present study is stronger than that in Lin et al., which is probably the main reason for the lower MAC value of toluene SOA observed in this study.

The $MAC_{\lambda=365\ nm}$ of toluene SOA generated in the study of Xie et al. was 0.17 and 0.55 $m^2\ g^{-1}$ under the lower and high NO_2 conditions, respectively. The $MAC_{\lambda=365\ nm}$ value observed by Lin et al. is consistent

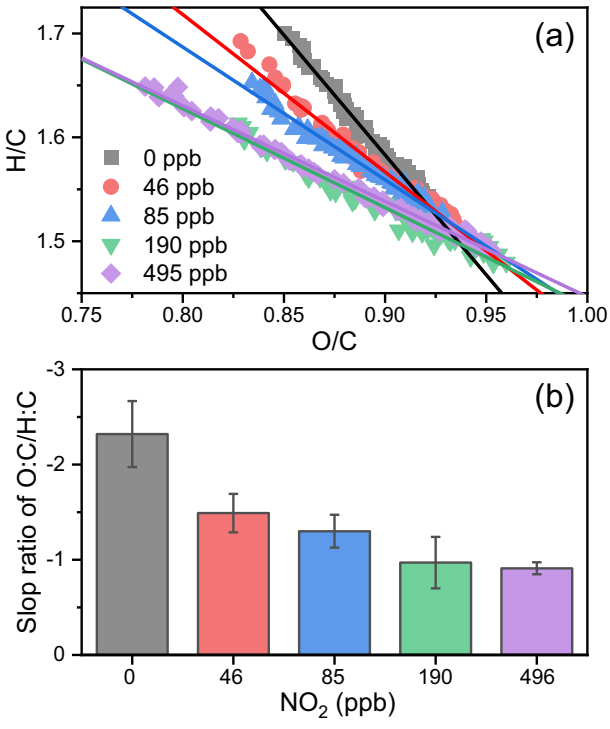

Fig. 3. The elemental ratios of O/C vs. H/C (a) and The fitted slope of O/C vs. H/C (b) for different initial NO_2 concentrations.

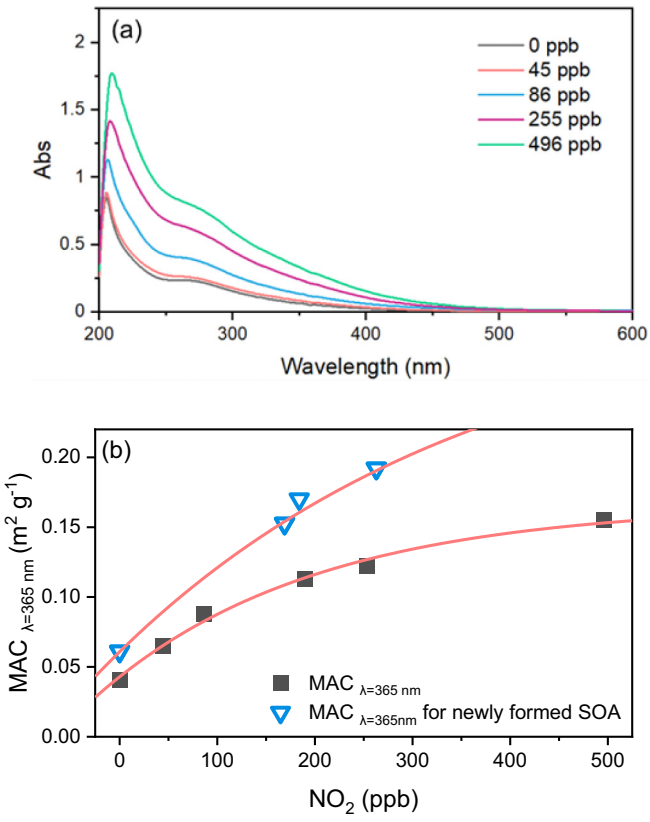

Fig. 4. Abs (a) and $MAC_{\lambda=365\ nm}$ (b) of the toluene-derived SOA with different initial NO_2 concentrations (The blue triangle points represent the $MAC_{\lambda=365\ nm}$ of newly formed SOA, the black square points represent the $MAC_{\lambda=365\ nm}$ of aged SOA with an average photooxidation time of 2 h).

Table 2
Relationship between $MAC_{\lambda=365\ nm}$ and initial NO_2 concentration for several chamber result.

	Light source	Seed particles	Low NO_2 condition		High NO_2 condition		
			$[NO_2]_0$ (ppbv)	$MAC_{\lambda=365\ nm}$ ($m^2\ g^{-1}$)	$[NO_2]_0$ (ppbv)	$[NO_2]_0/[toluene]_0$	$MAC_{\lambda=365\ nm}$ ($m^2\ g^{-1}$)
This study	UV light (254 nm)	No	No	0.03	496	1:1	0.15
Lin et al. (2015)	Black light (365 nm)	No	<2	0.01	1500	5:1	0.78
Xie et al. (2017)	Black light (365 nm)	$(NH_4)_2SO_4$	No	0.17	300	1:10	0.55

with that observed by Xie et al. at high NO_2 condition, but the initial NO_2 concentration and the $[NO_2]_0/[toluene]_0$ ratio under high NO_2 condition in Xie et al. were only 300 ppbv and 1:10, respectively, which are much lower than those of Lin et al. (Lin et al., 2015; Xie et al., 2017). The $MAC_{\lambda=365\ nm}$ value in the absence of NO_2 from Xie et al. study is much higher than the results from both Lin et al. and our study. Xie et al. reported that 4-nitrocatechol, 2-methyl-4-nitroresorcinol, and 2-nitrophloroglucinol were the main nitroaromatic compounds detected in the toluene/NO_2 SOA, but the contribution of nitroaromatic compounds absorption was only 13% to the light absorption coefficients of toluene SOA extracts at 365 nm, suggesting the formation of other types of absorbents, which resulted in the enhancement of the toluene SOA absorbance. Ammonium sulfate [$(NH_4)_2SO_4$] seed aerosol at a concentration of 0.1–1 μg m^{-3} was introduced for the experiments to promote SOA formation in the study of Xie et al. (2017). The heterogeneous reaction of ammonium with the carbonyl and carboxyl group from the toluene SOA could produce more NOCs, and enhance the absorbance of SOA (Qi et al., 2020). Therefore, the MAC value observed by Xie et al. (2017) under a very low ratio of NO_2 to toluene conditions is still comparable and even higher than that of the experiments with no $(NH_4)_2SO_4$ seeds such as the cases of Lin et al. (2015) and this study (Table 2).

3.3. Chemical composition of toluene-derived SOA

The molecular-level study of SOA chemistry is helpful for better understanding on the change of SOA yield and the evolution of light absorbing of the BrC. The typical mass spectrum from toluene-derived SOA with different initial NO_2 concentration is shown in Fig. 6. The fragments at *m/z* 28 (CO^+), 43 ($C_2H_3O^+$) from CHO family, and fragments m/z 44 (CO_2^+) from CHO_x (here x>1) family spectrum were dominant in the AMS spectrum. The relative intensity between m/z 43 and m/z 44 was one of the most significant changes of the AMS spectra obtained from different NO_2 conditions. The m/z 43 ion signal includes the fresh less-oxidized organic aerosols, while the m/z 44 ion signal is an indicator of highly oxygenated organic aerosols (Ng et al., 2010). The increasing relative intensity of m/z 44 indicated that the toluene SOA is more oxidized with increase NO_2 concentration, suggesting that the presence of NO_2 promotes the formation of some high oxidation state products containing more carboxyl groups, e.g., glyoxylic acid, through toluene photooxidation (Chhabra et al., 2010; Ng et al., 2010).

In the presence of NO_2, many N-containing fragments were observed in the AMS spectra. The total NOCs was detected as the CHN, CHON and CHO_xN fragment groups by the AMS. The dominated N-containing fragments from the CHN family were observed at m/z 27 (CHN^+), 41 ($C_2H_3N^+$), 41 ($C_2H_5N^+$), respectively, and the strong fragments from CHON and CHO_xN groups were also observed at m/z 44 (CH_2ON^+), 45 (CH_3ON^+), 73 ($C_3H_7ON^+$). As shown in Fig. 7, the content of total N-containing fragments in SOA were 2.5%, 2.9%, 4.3% and 6.0% with initial NO_2 concentrations of 45, 86, 190 and 495 ppbv, respectively. Some of the NOCs may fragment into ions that do not contain nitrogen atoms, and here were categorized into the groups of CH, CHO and

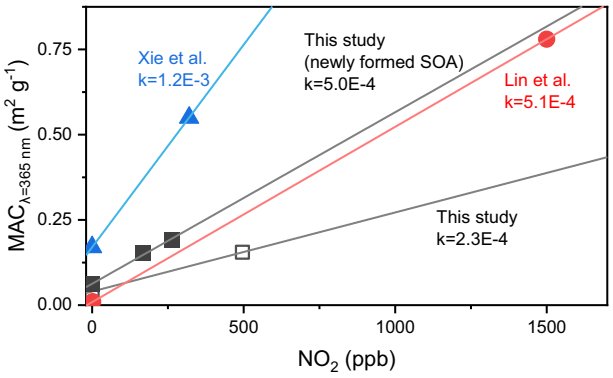

Fig. 5. The relationship between $MAC_{\lambda=365}$ nm and initial NO_2 concentration reported by different studies.

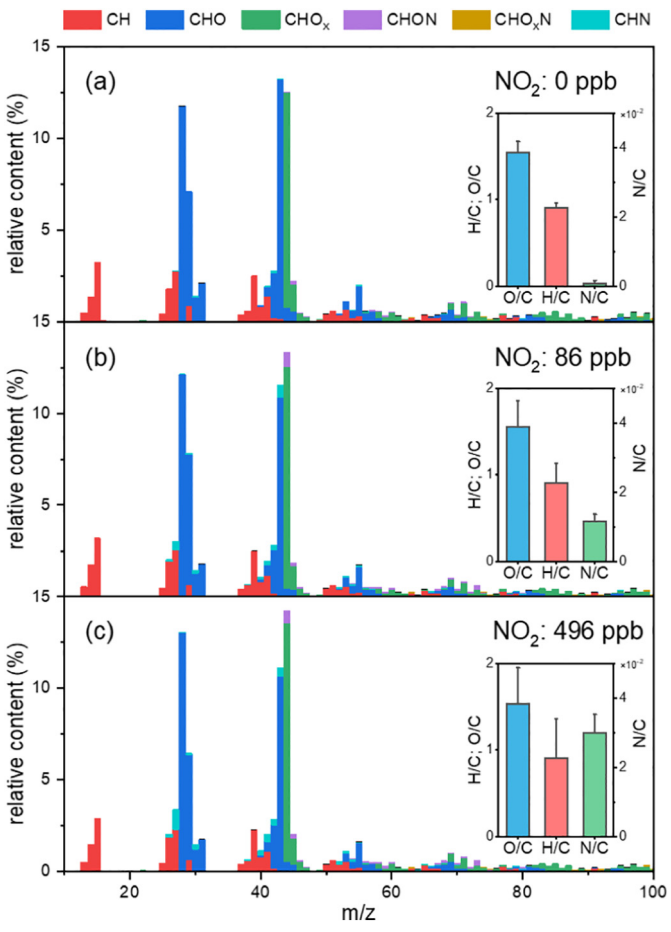

Fig. 6. The typical HR-ToF-AMS spectra of toluene-derived SOA with different concentration of initial NO_2. The figure inset shows the elemental ratios for different experiments.

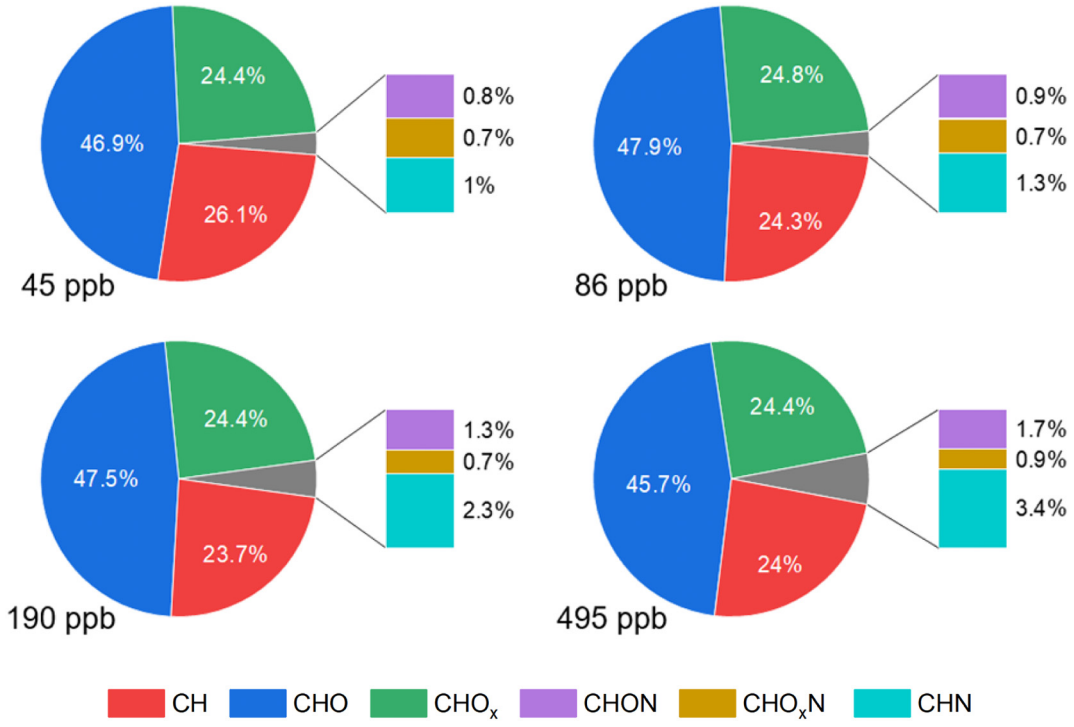

Fig. 7. Chemical composition of tolune-derived SOA with different initial NO_2 concentration measured by HR-ToF-AMS.

CHO_x. Thus, the concentration of total N-containing fragments in the SOA might be much lower than the concentration of NOCs.

Obviously, NO_2 could promote the formation of NOCs, although the signal intensities of N-containing fragments were weaker than those of the CH, CHO and CHO_x families. Yan et al. (2020) pointed out that the NOCs are strong BrC chromophores, and even a small amount of nitro-aromatic compounds could contribute significantly to the light absorption of particles (Yan et al., 2020). Fig. 8 shows the relationship between $MAC_{\lambda=365\ nm}$ and the content of N-containing fragments in the total SOA mass with different initial NO_2 concentration. The $MAC_{\lambda=365\ nm}$ was increasing linearly ($R^2 = 0.97$) with the concentration of N-containing fragments, clearly demonstrating that the nitrogen-containing functional groups are the important BrC chromophores and responsible for the enhanced light absorption of the toluene-derived SOA. We also attempted to link optical properties to the elemental ratios of chemical composition. We therefore investigated $MAC_{\lambda=365\ nm}$ versus N/C ratios in Fig. 8b. Indeed, the $MAC_{\lambda=365\ nm}$ value of toluene-derived SOA also appeared to increase in general with the increases of N/C ratios from AMS measurements, and there had strong correlations of $MAC_{\lambda=365\ nm}$ and N/C ratios. Chen et al. (2018) and Y.F. Chen et al. (2020) investigated the light absorption and chemical properties of BrC in $PM_{2.5}$ collected in field experiments, and a positive response of $MAC_{\lambda=365\ nm}$ to N/C ratios and organic nitrogen (ON) contents were observed, and these results also indicated that ON species are important BrC chromophores (Chen et al., 2018; Y.F. Chen et al., 2020).

However, when the content of N-containing fragments in the SOA increased, the relative proportion of different kind of NOCs also changed

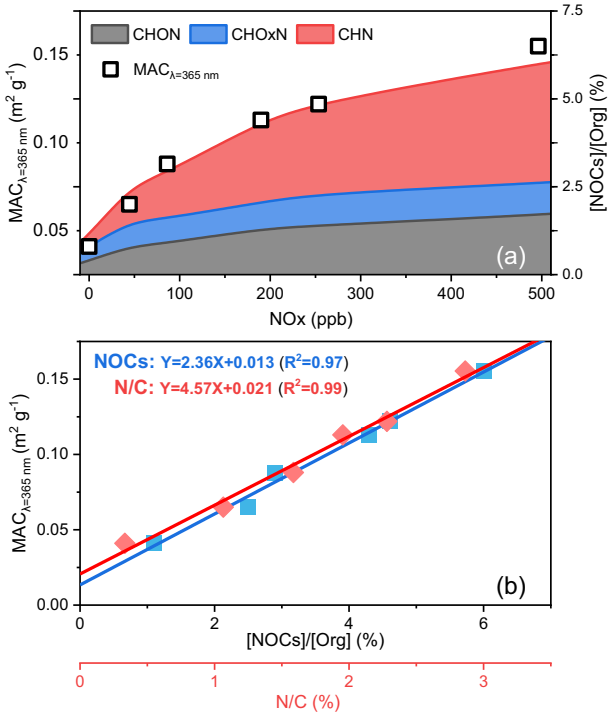

Fig. 8. The relationship between $MAC_{\lambda=365\ nm}$ and NOCs concentrations or N/C ratios in SOA with different initial NO_2 concentrations.

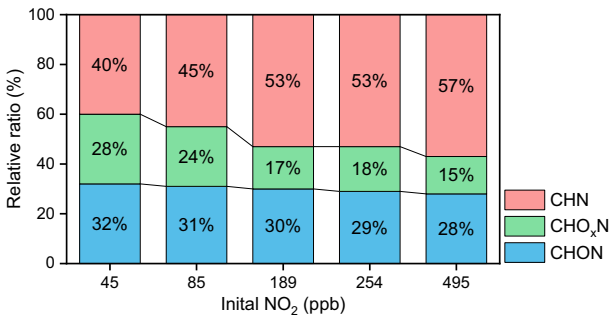

Fig. 9. The relative abundances of CHON, CHO_xN and CHN family fragments in the chamber under different initial NO_2 concentrations.

significantly. The ratio of fragment intensity of CHON, CHO_xN and CHN family at different NO_2 experiments is shown in Fig. 9. The proportion of CHN family in the N-containing fragments only accounted for 40% under the initial 45 ppbv NO_2 conditions. The proportion of CHN family increased with the initial NO_2 concentrations, and accounted for 57% of the NOC when the initial NO_2 concentration increased to 495 ppbv. The organonitrates are the important nitrogen components and widely found in the atmosphere (Li et al., 2018). C-O-N is the basic structure of organonitrogen molecules, where the C atom directly connects with the O atom. In contrast, for the CHN family, the C atom directly connects with the N atom. Hence, the fragments of CHN family are definitely not from the organonitrogen. Instead, they should come from the nitro compounds. Laboratory chamber studies have reported that the nitro compounds can be produced from the toluene SOA in the presence of NO_2 (Lin et al., 2015). Y. Wang et al. (2019) and X.R. Li et al. (2020) also reported that NO_2 plays important roles in the secondary formation of nitro-aromatic compounds via photooxidation of anthropogenic VOCs precursors (e.g., toluene, benzene) (Y. Wang et al., 2019; Yan et al., 2020). Nitro-aromatic compounds are of a strong light-absorbing ability (X.R. Li et al., 2020). Therefore, the increased relative

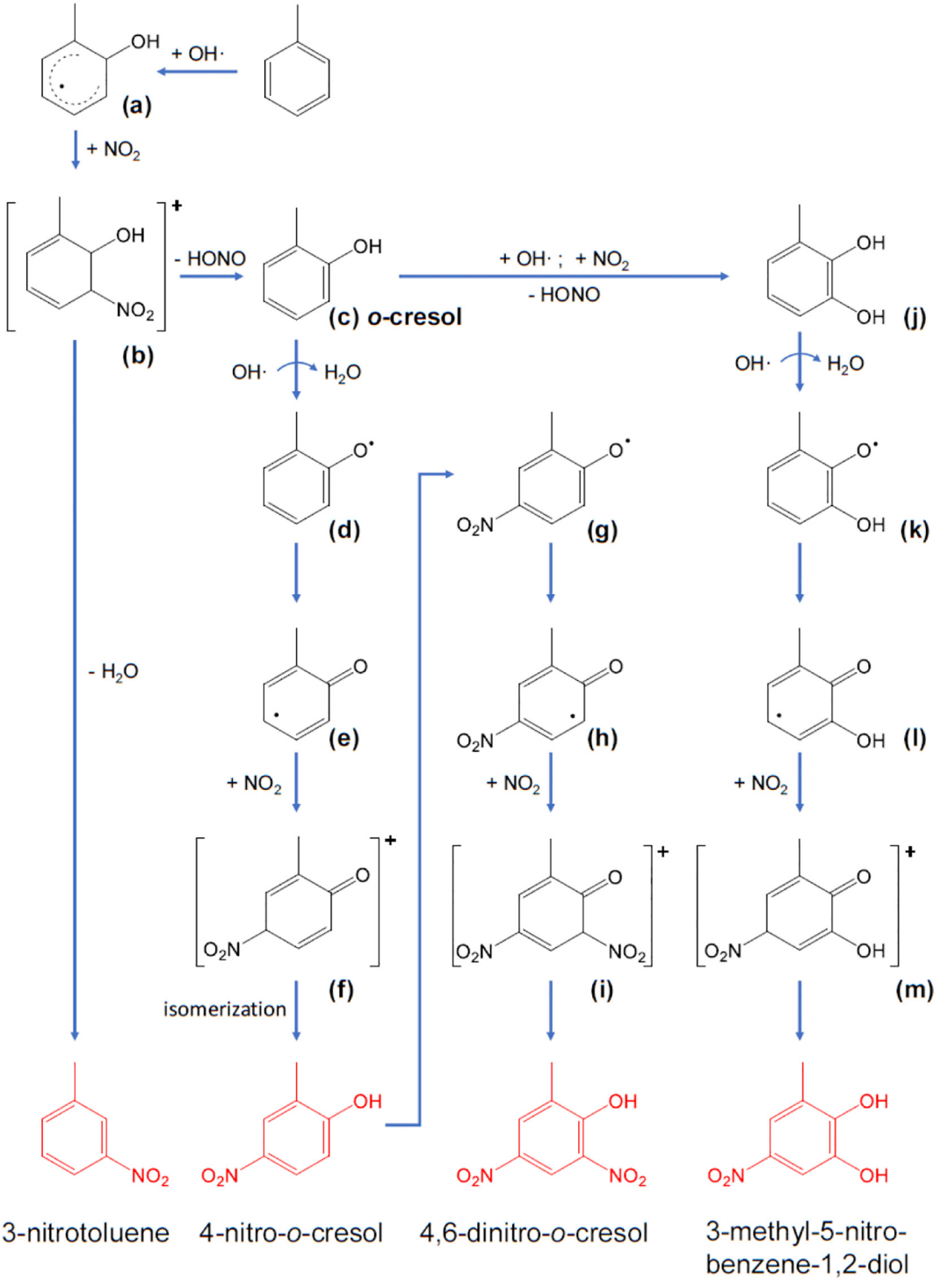

Fig. 10. Formation pathways of nitro-aromatic compounds in toluene photooxidation in the presence of NO_2.

abundance of nitro compounds, i.e., the CHN family, to the total NOCs can explain the enhanced light absorbance of SOA under the high NO_2 conditions.

The mechanism of nitro compounds formation from photooxidation in the presence of NO_2 is discussed here (Fig. 10). Toluene is known to react with OH to form the OH-aromatic adduct (a), which can react with O_2 or NO_2 (Hurley et al., 2001). According to the rate constant for reaction of OH-adduct with NO_2 ($k = 3.6 \pm 0.4 \times 10^{-11}$ cm^3 $molecule^{-1}$ s^{-1}) and with O_2 ($k = 2.28 \pm 0.34 \times 10^{-16}$ cm^3 $molecule^{-1}$ s^{-1}), 28% of OH-aromatic adduct could be consumed through the reaction of adduct + NO_2 when the initial NO_2 concentration increased to the maximum of 496.2 ppbv in this study. The 3-nitrotoluene is believed to be produced by the reaction of OH-aromatic adduct with NO_2 (Sato et al., 2007). Ji et al. (2017) revealed that the *o*-cresol (c) formation represented the dominant pathway for toluene OH oxidation (Ji et al., 2017). A methylphenoxy radical (d) was formed as an intermediate product in the reaction between OH and *o*-cresol. The NO_2 added to the benzene ring of methylphenoxy radical could form another adduct (f), which would form the 4-nitro-*o*-cresols through the isomerization reactions (Jang and Kamens, 2001). Nitrocresols are produced as the second-generation products. The 3-methylbenzene-1,2-diol (j) would further react into *o*-cresol. Because the molecular structure of both 4-nitro-*o*-cresol and 3-methylbenzene-1,2-diol are similar to *o*-cresol, another nitro group was added to the benzene ring by the reaction of 4-nitro-*o*-cresol or 3-methylbenzene-1,2-diol with OH radicals in the presence of NO_2 in the similar process to form 4,6-dinitro-*o*-cresol and 3-methyl-5-nitrobenzene-1,2-diol. All these nitro-aromatic compounds have been observed in field studies (Y. Wang et al., 2019). In addition to the nitro-aromatic compounds detected by the AMS, the formation of linear chain or branched-chain nitro compounds may also occur during the reaction. Future studies are necessary to identify the exact chemical formula of nitro compounds via a liquid chromatography-electrospray ionization multistage mass spectrometry (LC-ESI-MS).

4. Conclusion

The production yield and light absorption of toluene SOA from OH photooxidation in the presence of NO_2 was studied by using a chamber simulation technique. The SOA concentration first increased with the initial NO_2 concentration below 100 ppbv, and maximized at a value of 146.4 ± 1.8 μg m^{-3}. Then, the SOA concentration decreased slowly along with the continuous increase in initial concentrations of NO_2. Both the acid-catalyzed reaction by nitric acid and the formation of lower volatile compounds (e.g., glyoxylic acid) are responsible for the increase of the SOA yield.

HR-ToF-AMS results showed that the presence of NO_2 enhanced the light absorption of toluene SOA by forming NOCs. The ratio of NOCs to the total SOA increased with an increase of initial NO_2 concentrations, and showed a robust linear correlation with $MAC_{\lambda=365\ nm}$, suggesting a dominant contribution of NOCs to the light absorption of secondary BrC produced from toluene photooxidation. HR-ToF-AMS characterization further revealed that nitro-aromatic compounds are the major light-absorbing compounds and dominant in NOCs at high NO_2 concentration with organonitrogen being relatively minor.

CRediT authorship contribution statement

SL and GW conceived the experiment. SL and YW performed the experiment. SL, GW conducted the data interpretation and wrote the paper. SZ, DL, LD, CW, WD and SG contributed useful discussions and comments.

Declaration of competing interest

We declare that we have no known competing financial interests or personal relationships that could have appeared to influence the work reported in this paper.

Acknowledgements

This work was financially supported by National Key Research and Development Program (Grant No. 2017YFC0212703); National Natural Science Foundation of China (Grant Nos. 41773117, 42005088); the China Postdoctoral Science Foundation (Grant No. 2019M661427); Fundamental Research Funds for the Central Universities, Director's Fund of Key Laboratory of Geographic Information Science (Ministry of Education), East China Normal University (Grant No. KLGIS2021C02); and ECNU Happiness Flower Program.

We thank Mrs. Lijuan Li and Prof. Jianjun Li from the Institute of Earth Environment, Chinese Academy of Sciences for their helpful discussion on the AMS data analysis.

References

Boyd, C.M., Sanchez, J., Xu, L., Eugene, A.J., Nah, T., Tuet, W.Y., et al., 2015. Secondary organic aerosol formation from the β-pinene+NO_3 system: effect of humidity and peroxy radical fate. Atmos. Chem. Phys. 15, 7497–7522.

Chen, Y., Li, N., Li, X., Tao, Y., Luo, S., Zhao, Z., et al., 2020a. Secondary organic aerosol formation from $^3C^*$-initiated oxidation of 4-ethylguaiacol in atmospheric aqueous-phase. Sci. Total Environ. 723, 137953.

Chen, Y.F., Ge, X.L., Chen, H., Xie, X.C., Chen, Y.T., Wang, J.F., et al., 2018. Seasonal light absorption properties of water-soluble brown carbon in atmospheric fine particles in Nanjing, China. Atmos. Environ. 187, 230–240.

Chen, Y.F., Xie, X.C., Shi, Z., Li, Y.L., Gai, X.Y., Wang, J.F., et al., 2020b. Brown carbon in atmospheric fine particles in Yangzhou, China: Light absorption properties and source apportionment. Atmos. Res. 244, 105028.

Chhabra, P.S., Flagan, R.C., Seinfeld, J.H., 2010. Elemental analysis of chamber organic aerosol using an aerodyne high-resolution aerosol mass spectrometer. Atmos. Chem. Phys. 10, 4111–4131.

Chhabra, P.S., Ng, N.L., Canagaratna, M.R., Corrigan, A.L., Russell, L.M., Worsnop, D.R., et al., 2011. Elemental composition and oxidation of chamber organic aerosol. Atmos. Chem. Phys. 11, 8827–8845.

Chung, C.E., Ramanathan, V., Decremer, D., 2012. Observationally constrained estimates of carbonaceous aerosol radiative forcing. Proc. Natl. Acad. Sci. U. S. A. 109, 11624–11629.

Connelly, B.M., De Haan, D.O., Tolbert, M.A., 2012. Heterogeneous glyoxal oxidation: a potential source of secondary organic aerosol. J. Phys. Chem. A 116, 6180–6187.

Farmer, D.K., Matsunaga, A., Docherty, K.S., Surratt, J.D., Seinfeld, J.H., Ziemann, P.J., et al., 2010. Response of an aerosol mass spectrometer to organonitrates and organosulfates and implications for atmospheric chemistry. Proc. Natl. Acad. Sci. U. S. A. 107, 6670–6675.

Fry, J.L., Draper, D.C., Zarzana, K.J., Campuzano-Jost, P., Day, D.A., Jimenez, J.L., et al., 2013. Observations of gas- and aerosol-phase organic nitrates at BEACHON-RoMBAS 2011. Atmos. Chem. Phys. 13, 8585–8605.

Ge, S., Wang, G., Zhang, S., Li, D., Xie, Y., Wu, C., et al., 2019. Abundant NH_3 in China enhances atmospheric HONO production by promoting the heterogeneous reaction of SO_2 with NO_2. Environ. Sci. Technol. 53, 14339–14347.

Han, T., Qiao, L., Zhou, M., Qu, Y., Du, J., Liu, X., et al., 2015. Chemical and optical properties of aerosols and their interrelationship in winter in the megacity Shanghai of China. J. Environ. Sci. 27, 59–69.

Hu, D., Tolocka, M., Li, Q., Kamens, R.M., 2007. A kinetic mechanism for predicting secondary organic aerosol formation from toluene oxidation in the presence of NOx and natural sunlight. Atmos. Environ. 41, 6478–6496.

Huang, D.D., Zhang, Q., HHY, Cheung, Yu, L., Zhou, S., Anastasio, C., et al., 2018. Formation and evolution of aqSOA from aqueous-phase reactions of phenolic carbonyls: comparison between ammonium sulfate and ammonium nitrate solutions. Environ. Sci. Technol. 52, 9215–9224.

Hurley, M.D., Sokolov, O., Wallington, T.J., Takekawa, H., Karasawa, M., Klotz, B., et al., 2001. Organic aerosol formation during the atmospheric degradation of toluene. Environ. Sci. Technol. 35, 1358–1366.

Jang, M., Kamens, R.M., 2001. Characterization of secondary aerosol from the photooxidation of toluene in the presence of NOx and 1-propene. Environ. Sci. Technol. 35, 3626–3639.

Jang, M., Czoschke, N.M., Lee, S., Kamens, R.M., 2002. Heterogeneous atmospheric aerosol production by acid-catalyzed particle-phase reactions. Science 298, 814–817.

Ji, Y., Zhao, J., Terazono, H., Misawa, K., Levitt, N.P., Li, Y., et al., 2017. Reassessing the atmospheric oxidation mechanism of toluene. Proc. Natl. Acad. Sci. U. S. A. 114, 8169–8174.

Jo, D.S., Park, R.J., Lee, S., Kim, S.W., Zhang, X., 2016. A global simulation of brown carbon: implications for photochemistry and direct radiative effect. Atmos. Chem. Phys. 16, 3413–3432.

Laskin, A., Laskin, J., Nizkorodov, S.A., 2015. Chemistry of atmospheric brown carbon. Chem. Rev. 115, 4335–4382.

Laskin, J., Laskin, A., Roach, P.J., Slysz, G.W., Anderson, G.A., Nizkorodov, S.A., et al., 2010. High-resolution desorption electrospray ionization mass spectrometry for chemical characterization of organic aerosols. Anal. Chem. 82, 2048–2058.
Li, J., Zhang, Q., Wang, G., Li, J., Wu, C., Liu, L., et al., 2020a. Optical properties and molecular compositions of water-soluble and water-insoluble brown carbon (BrC) aerosols in northwest China. Atmos. Chem. Phys. 20, 4889–4904.
Li, R., Wang, X.F., Gu, R.R., Lu, C.Y., Zhu, F.P., Xue, L.K., et al., 2018. Identification and semi-quantification of biogenic organic nitrates in ambient particulate matters by UHPLC/ESI-MS. Atmos. Environ. 176, 140–147.
Li, X.R., Yang, Y., Liu, S.Q., Zhao, Q., Wang, G.H., Wang, Y.S., 2020b. Light absorption properties of brown carbon (BrC) in autumn and winter in Beijing: composition, formation and contribution of nitrated aromatic compounds. Atmos. Environ. 223, 117289.
Lin, G.X., Penner, J.E., Flanner, M.G., Sillman, S., Xu, L., Zhou, C., 2014a. Radiative forcing of organic aerosol in the atmosphere and on snow: effects of SOA and brown carbon. J. Geophys. Res.-Atmos. 119, 7453–7476.
Lin, P., Liu, J., Shilling, J.E., Kathmann, S.M., Laskin, J., Laskin, A., 2015. Molecular characterization of brown carbon (BrC) chromophores in secondary organic aerosol generated from photo-oxidation of toluene. Phys. Chem. Chem. Phys. 17, 23312–23325.
Lin, Y.H., Budisulistiorini, S.H., Chu, K., Siejack, R.A., Zhang, H., Riva, M., et al., 2014b. Light-absorbing oligomer formation in secondary organic aerosol from reactive uptake of isoprene epoxydiols. Environ. Sci. Technol 48, 12012–12021.
Liu, P.F., Abdelmalki, N., Hung, H.M., Wang, Y., Brune, W.H., Martin, S.T., 2015a. Ultraviolet and visible complex refractive indices of secondary organic material produced by photooxidation of the aromatic compounds toluene and m-xylene. Atmos. Chem. Phys. 15, 1435–1446.
Liu, S.J., Jia, L., Xu, Y., Tsona, N.T., Ge, S.S., Du, L., 2017. Photooxidation of cyclohexene in the presence of SO_2: SOA yield and chemical composition. Atmos. Chem. Phys. 17, 13329–13343.
Liu, S.J., Jiang, X.T., Tsona, N.T., Lv, C., Du, L., 2019. Effects of NOx, SO_2 and RH on the SOA formation from cyclohexene photooxidation. Chemosphere 216, 794–804.
Liu, Y.C., Liggio, J., Staebler, R., Li, S.M., 2015b. Reactive uptake of ammonia to secondary organic aerosols: kinetics of organonitrogen formation. Atmos. Chem. Phys. 15, 13569–13584.
Ma, P., Zhang, P., Shu, J., Yang, B., Zhang, H., 2018. Characterization of secondary organic aerosol from photo-oxidation of gasoline exhaust and specific sources of major components. Environ. Pollut. 232, 65–72.
Ma, Y.Q., Cheng, Y.B., Qiu, X.H., Cao, G., Kuang, B.Y., Yu, J.Z., et al., 2019. Optical properties, source apportionment and redox activity of humic-like substances (HULIS) in airborne fine particulates in Hong Kong. Environ. Pollut. 255, 9.
Middlebrook, A.M., Bahreini, R., Jimenez, J.L., Canagaratna, M.R., 2012. Evaluation of composition-dependent collection efficiencies for the aerodyne aerosol mass spectrometer using field data. Aerosol Sci. Technol. 46, 258–271.
Ng, N.L., Kroll, J.H., Chan, A.W.H., Chhabra, P.S., Flagan, R.C., Seinfeld, J.H., 2007. Secondary organic aerosol formation from m-xylene, toluene, and benzene. Atmos. Chem. Phys. 7, 3909–3922.
Ng, N.L., Canagaratna, M.R., Zhang, Q., Jimenez, J.L., Tian, J., Ulbrich, I.M., et al., 2010. Organic aerosol components observed in northern hemispheric datasets from aerosol mass spectrometry. Atmos. Chem. Phys. 10, 4625–4641.
Ng, N.L., Brown, S.S., Archibald, A.T., Atlas, E., Cohen, R.C., Crowley, J.N., et al., 2017. Nitrate radicals and biogenic volatile organic compounds: oxidation, mechanisms, and organic aerosol. Atmos. Chem. Phys. 17, 2103–2162.
Peng, C., Yang, F., Tian, M., Shi, G., Li, L., Huang, R.J., et al., 2020. Brown carbon aerosol in two megacities in the Sichuan Basin of southwestern China: light absorption properties and implications. Sci. Total Environ. 719, 137483.
Qi, X., Zhu, S., Zhu, C., Hu, J., Lou, S., Xu, L., et al., 2020. Smog chamber study of the effects of NOx and NH_3 on the formation of secondary organic aerosols and optical properties from photo-oxidation of toluene. Sci. Total Environ. 727, 138632.
Sarrafzadeh, M., Wildt, J., Pullinen, I., Springer, M., Kleist, E., Tillmann, R., et al., 2016. Impact of NOx and OH on secondary organic aerosol formation from β-pinene photooxidation. Atmos. Chem. Phys. 16, 11237–11248.
Sato, K., Hatakeyama, S., Imamura, T., 2007. Secondary organic aerosol formation during the photooxidation of toluene: NOx dependence of chemical composition. J. Phys. Chem. A 111, 9796–9808.
Sato, K., Takami, A., Isozaki, T., Hikida, T., Shimono, A., Imamura, T., 2010. Mass spectrometric study of secondary organic aerosol formed from the photo-oxidation of aromatic hydrocarbons. Atmos. Environ. 44, 1080–1087.
Slikboer, S., Grandy, L., Blair, S.L., Nizkorodov, S.A., Smith, R.W., Al-Abadleh, H.A., 2015. Formation of light absorbing soluble secondary organics and insoluble polymeric particles from the dark reaction of catechol and guaiacol with Fe(III). Environ. Sci. Technol. 49, 7793–7801.
Wang, G., Zhang, R., Gomez, M.E., Yang, L., Levy Zamora, M., Hu, M., et al., 2016. Persistent sulfate formation from London Fog to Chinese haze. Proc. Natl. Acad. Sci. U. S. A. 113, 13630–13635.
Wang, J., Ye, J., Zhang, Q., Zhao, J., Wu, Y., Li, J., et al., 2021. Aqueous production of secondary organic aerosol from fossil-fuel emissions in winter Beijing haze. Proc. Natl. Acad. Sci. U. S. A. 118, e2022179118.
Wang, Q.Y., Han, Y.M., Ye, J.H., Liu, S.X., Pongpiachan, S., Zhang, N.N., et al., 2019a. High contribution of secondary brown carbon to aerosol light absorption in the southeastern margin of Tibetan Plateau. Geophys. Res. Lett. 46, 4962–4970.
Wang, X., Heald, C.L., Liu, J.M., Weber, R.J., Campuzano-Jost, P., Jimenez, J.L., et al., 2018. Exploring the observational constraints on the simulation of brown carbon. Atmos. Chem. Phys. 18, 635–653.
Wang, Y., Hu, M., Wang, Y., Zheng, J., Shang, D., Yang, Y., et al., 2019b. The formation of nitro-aromatic compounds under high NOx and anthropogenic VOC conditions in urban Beijing. China. Atmos. Chem. Phys 19, 7649–7665.
Wu, G.M., Wan, X., Ram, K., Li, P.L., Liu, B., Yin, Y.G., et al., 2020. Light absorption, fluorescence properties and sources of brown carbon aerosols in the Southeast Tibetan Plateau. Environ. Pollut. 257 (12).
Xie, M., Chen, X., Hays, M.D., Lewandowski, M., Offenberg, J., Kleindienst, T.E., et al., 2017. Light absorption of secondary organic aerosol: composition and contribution of nitroaromatic compounds. Environ. Sci. Technol. 51, 11607–11616.
Xu, J., Cui, T.Q., Fowler, B., Fankhauser, A., Yang, K., Surratt, J.D., et al., 2018. Aerosol brown carbon from dark reactions of syringol in aqueous aerosol mimics. Acs Earth Space Chem 2, 608–617.
Xu, J.L., Griffin, R.J., Liu, Y., Nakao, S., Cocker, D.R., 2015a. Simulated impact of NOx on SOA formation from oxidation of toluene and m-xylene. Atmos. Environ. 101, 217–225.
Xu, L., Suresh, S., Guo, H., Weber, R.J., Ng, N.L., 2015b. Aerosol characterization over the southeastern United States using high-resolution aerosol mass spectrometry: spatial and seasonal variation of aerosol composition and sources with a focus on organic nitrates. Atmos. Chem. Phys. 15, 7307–7336.
Xu, L., Moller, K.H., Crounse, J.D., Kjaergaard, H.G., Wennberg, P.O., 2020. New insights into the radical chemistry and product distribution in the OH-initiated oxidation of benzene. Environ. Sci. Technol. 54, 13467–13477.
Yan, C., Zheng, M., Desyaterik, Y., Sullivan, A., Wu, Y.S., Collett, J.L., 2020. Molecular characterization of water-soluble brown carbon chromophores in Beijing. China. J. Geophys. Res.-Atmos. 125, 18.
Zhang, A.X., Wang, Y.H., Zhang, Y.Z., Weber, R.J., Song, Y.J., Ke, Z.M., et al., 2020. Modeling the global radiative effect of brown carbon: a potentially larger heating source in the tropical free troposphere than black carbon. Atmos. Chem. Phys. 20, 1901–1920.
Zhang, Y.Z., Forrister, H., Liu, J.M., Dibb, J., Anderson, B., Schwarz, J.P., et al., 2017. Top-of-atmosphere radiative forcing affected by brown carbon in the upper troposphere. Nat. Geosci. 10, 486–489.
Zhao, D.F., Schmitt, S.H., Wang, M.J., Acir, I.H., Tillmann, R., Tan, Z.F., et al., 2018. Effects of NOx and SO_2 on the secondary organic aerosol formation from photooxidation of α-pinene and limonene. Atmos. Chem. Phys. 18, 1611–1628.
Zou, Y., Deng, X.J., Zhu, D., Gong, D.C., Wang, H., Li, F., et al., 2015. Characteristics of 1 year of observational data of VOCs, NOx and O_3 at a suburban site in Guangzhou. China. Atmos. Chem. Phys 15, 6625–6636.